# ENHANCED BROADBAND TRI-STABLE ENERGY HARVESTING SYSTEM
# BY ADAPTING POTENTIAL ENERGY – EXPERIMENTAL STUDY

**Andrzej KOSZEWNIK\* , Bartłomiej AMBROŻKIEWICZ\*\***

\*Faculty of Mechanical Engineering, Bialystok University of Technology,
Wiejska 45C Street, 15-351 Białystok, Poland
\*\*Faculty of Mathematics and Information Technology, Lublin University of Technology,
Nadbystrzycka 38 Street, 20-618 Lublin, Poland

a.koszewnik@pb.edu.pl, b.ambrozkiewicz@pollub.pl

**Abstract:** This paper presents the process optimization of some key parameters, such as the size of the air gap and distance between fixed neodymium magnets to enhance the vibration-based energy harvesting effect in the tri-stable energy harvesting systems and the improved tri-stable energy harvesting system being the proposed solution under weak excitation. In order to do it, firstly the distributed parameters model of the magnetic coupling energy harvesting system, including macro fiber composites of the 8514 P2 with a homogenous material in the piezoelectric fiber layer and nonlinear magnetic force, was determined. The performed numerical analysis of the conventional and the improved tri-stable energy harvesting system indicated that introducing an additional magnet to the tri-stable system leads to the shallowing of the depth of a potential well by decreasing the air gap between magnets and consequently generating higher power output and improving the effectiveness of the proposed improved tri-stable energy harvesting system. Experiments carried out on the laboratory stand allowed us to verify the numerical results as well as determine the optimal parameters of the magnetic coupling system. Due to it, the effectiveness of the proposed system versus the conventional tri-stable energy harvesting system is most enhanced.

**Keywords:** macro-fiber composite, homogenized material, conventional TPEH, improved TPEH system, tailoring potential energy

## 1. INTRODUCTION

Low-power sensor systems and wireless networks typically rely on external energy sources, but batteries present challenges like short lifespan and bulkiness. To address this, researchers are increasingly focused on harvesting energy from the ambient environment, particularly from mechanical vibrations, to provide continuous power for low-power devices [1-4]. Piezoelectric cantilever harvesters offer advantages like simplicity, high energy density, and no startup power. However, they are sub-optimal under variable frequencies and wideband vibrations, generating maximum energy only at the resonance frequency [3-5]. In order to obtain a wide spectrum response and adapt the harvester to the vibration source, a nonlinear piezoelectric cantilever energy harvester with an external magnetic field has been investigated [6-8]. Exemplary research, where a bi-stable generator was conducted and described, is presented in the paper written by Cottone [9]. In this paper, the authors demonstrated that the bi-stable piezoelectric energy harvesting (BPEH) system can overcome the limitations of linear harvesters and provide much more energy. In other papers written by Stanton [10] and Ferrari [11], the authors proved that BPEH systems can generate high output voltage due to the broadband effect. In order to broaden the bandwidth of BPEHs, other authors proposed a magnetic coupled piezoelectric energy harvester by introducing a magnetic oscillator to enhance the output power at relatively low excitation [12]. Although these methods somewhat enhance the performance of the BPEH sys-

tem, the governing energy functions are intrinsically bi-stable, which limits further improvement of output performances. Currently, tri-stable energy harvesters have attracted researchers' interest [13]. The prototype of these considerations is discussed in a paper written by Zhou and his group, who proposed a tri-stable piezoelectric energy harvester (TPEH) with two rotatable external magnets [14]. Simulations and experiments were conducted at different harmonic excitation levels, which proved wider-range frequencies of energy output. Then, they used Genetic Algorithms to identify the parameters of the EH system and verified the TPEH system can achieve higher values of the output energy [15]. In another paper, Cao et al [16] analyzed the influence of the energy potential well depth on the energy harvesting performance and they indicated that a shallower potential well depth will enhance the effective frequency width under low-frequency excitations. Another paper by Kim et al. [17,18] explored a cantilever-based magnetically coupled TPEH system. The results obtained allowed us to claim the advantages of the TPEH in broadband vibration energy harvesting under low-level excitations. Similar results were presented in a paper [19] where the authors explored the influence of the fractional-order viscoelastic material on the energy harvesting performances of the TPEH system. Yet another examples are papers [20,21], where TPEH is used to harvest energy from random excitations [22], while in [23] nonlinear magnetic force model for the magnetic coupled EH system was theoretically presented and experiment-tally verified to enhance the harvesting effect.

The review suggests that TPEH systems hold an advantage over BPEH systems, particularly in achieving higher efficiency through excitation with large amplitude vibrations. To address the efficiency maintenance, an improved tri-stable energy harvesting system is proposed in this paper. Considering an additionally fixed magnet with a low magnetic moment in the proposed EH system with a micro-fiber composite (MFC) element, consisting of homogenized material in the active layer, in contrast to [24,25], allows adapting  the potential energy shaper, especially under weak random excitations. This effect can be achieved by improving the electromechanical properties of this composite, which is a result of considering the multiphase construction of the MFC element   (thin piezoelectric fibers mixed with a softer passive epoxy material) [3, 26, 27, 28, 29]. As a result, such considered structure and the proposed EH system connected with an innovative storing unit containing a reed switch or a synchronized switch, harvesting on inductor units allow faster and better powering of small electrical devices with a lower power demand [30]. Taking into account this fact and to show the novelty of this paper, related to using the MFC element with homogenized material in the active layer, the manuscript is organized as follows. The electromechanical model of the magnetic coupled energy harvesting system as well as a model of nonlinear magnetic force in the TPEH and improved tri-stable piezoelectric energy harvester (ITPEH) systems derived by using the magnetization current method are described in Section 2. In Section 3, the numerical simulations are derived to compare the performances of TPEH and ITPEH systems in the form of potential energy diagrams are presented. Next, in Section 4, experimental investigations of both systems carried out in the lab stand on various initial parameters are presented and the results obtained are discussed. In addition, the Poincare maps analysis of both systems in this section are performed. Section 5 concludes the main findings of this work.

## 2. THE TRI-STABLE AND IMPROVED TRI-STABLE PIEZOELECTRIC ENERGY HARVESTING SYSTEM MODELING

In Fig.1a, a conventional tri-stable piezoelectric energy harvesting system, composed of a piezoelectric cantilever beam is presented. Magnet A was located on the free end of this beam, and two fixed external magnets, B and C, located on the frame. Under ambient vibrations or random excitation, the beam oscillations lead to deformation of the piezo-composite and convert the mechanical energy into electrical energy via the piezoelectric effect.

The difference between the tri-stable (TPEH) and bi-stable (BPEH) piezoelectric energy harvesting systems is related to the number of fixed external magnets. Similarly, in the case of the improved TPEH system, where the additional magnet located on the base between external magnets, is also considered (see Fig.1b). In this configuration, the ITPEH system has three magnets separated by a distance of $x_3$ (being one half of distance $x_1$ related to a conventional TPEH system), which are repelled by magnet A at the  free end of the beam located in a distance $x_2$. As a result, such modified configurations of the TPEH system lead to the increase of the potential energy in the middle well potential and, consequently, to improve the output performances of this system, which will be presented in the next Sections of this paper.

Taking into account the review of papers [17,18], as well as considering the case of the TPEH and ITPEH systems [24-33], the

governing equation of the electromechanical model of vibration energy harvesters is shown in Fig.2, and it can be written in the following form:

$$M_{eq}\ddot{x}(t) + C_{eq}\dot{x}(t) + K_{eq}\dot{x}(t) + F_m(x) - \theta_0 v(t) = F \cdot cos(\omega t)$$
$$C_p\dot{v}(t) + \frac{v(t)}{R_L} + \theta_0 \dot{x}(t) = 0 \qquad (1)$$

where: $M_{eq}$ – the equivalent mass, $C_{eq}$ – the equivalent damping, $C_{eq}$ – the equivalent stiffness, $C_p$ – the equivalent capacitance, $R_L$- the load resistance, $\theta_0$ – the electromechanical coupling factor, $v(t)$ – the voltage output across by the resistive load, $Fcos(\omega t)$ – the equivalent external excitation force (F=$\mu M_{eq}F_0$, $\mu$ – the amplitude-wise correction factor *while $F_0$ – the amplitude of base acceleration excitation)*, $F_m(x)$ – the nonlinear equivalent magnetic force, $x(t)$ – transverse deflection of a cantilever beam.
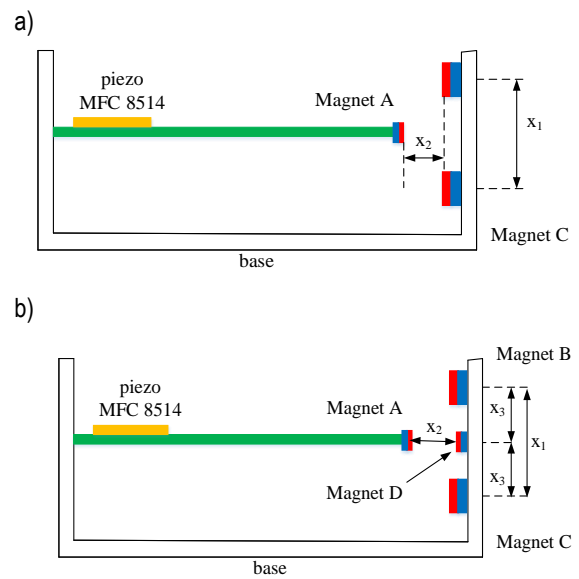


**Fig.1** The scheme of a) conventional tri-stable piezoelectric energy harvesting (TPEH) system, b) improved tri-stable piezoelectric energy harvesting (ITPEH) system
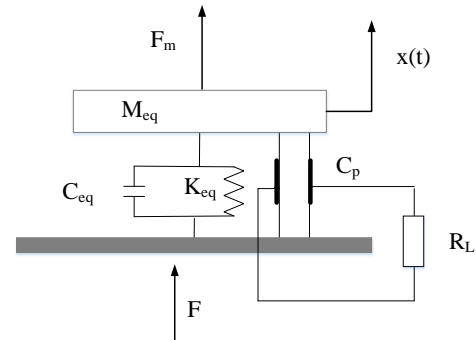


**Fig. 2.** The equivalent model of the coupled magnetic piezoelectric energy harvesting system

Then, considering also the approximated form of a magnetic force Fm(x) expressed in the form:

$$F_m(x) = \omega_0{}^2 x(t) + a_1 x(t)^3 + a_2 x(t)^5 + a_3 x(t)^7 \qquad (2)$$

where $\omega_0{}^2$, $a_{10}$, $a_{20}$, and $a_{30}$ are coefficients, which determines the electromechanical equation of both TPEH and IPTEH systems

rewritten in the following form:

$$\ddot{x}(t) + \frac{C}{M_{eq}}\dot{x}(t) + \frac{\omega_0^2}{M_{eq}}x(t) + \frac{a_{10}}{M_{eq}}x(t)^3 + \frac{a_{20}}{M_{eq}}x(t)^5 +$$

$$\frac{a_{30}}{M_{eq}}x(t)^7 - \frac{\theta_0}{M_{eq}}v(t) = \mu F_0 \cdot cos(\omega t)$$

$$\dot{v}(t) + \frac{v(t)}{C_p R_L} + \frac{\theta_0}{C_p}\dot{x}(t) = 0 \tag{3}$$

Moreover, introducing non-dimensional parameters listed below

$$c = \frac{C_{eq}}{M_{eq}}, \theta = \frac{\theta_0}{M_{eq}}, \omega^2 = \frac{\omega_0^2}{M_{eq}}, f = \frac{\mu F_0}{M_{eq}}, \lambda = \frac{1}{R_L C_p},$$

$$g = \frac{\theta_0}{C_p} a_1 = \frac{a_{10}}{M_{eq}}, \ a_2 = \frac{a_{20}}{M_{eq}}, \ a_3 = \frac{a_{30}}{M_{eq}}$$

The following non-dimensional governing electromechanical model can be expressed as:

$$\ddot{x}(t) + c\dot{x}(t) + \omega^2 x(t) + a_1 x(t)^3 + \ldots$$

$$+ a_2 x(t)^5 + a_3 x(t)^7 - \theta v(t) = f \cdot cos(\omega t)$$

$$\dot{v}(t) + \lambda v(t) + g\dot{x}(t) = 0 \tag{4}$$

## 3. POTENTIAL ENERGY AND MAGNETIC FORCE

The conducted analysis of the TPEH system and the performed simulations of the tri-stable energy harvesting system described in [1,8] indicated that one of the bigger difficulties is calculating the magnetic force $Fm$ which is closely related to the system design and performances of the magnetic coupling energy harvesting systems. Considering the findings [8], it is known that choosing appropriate magnets and their interval is of great importance to give the cantilever a higher transition probability. The mentioned problem for the conventional tri-stable piezoelectric EH system, as well as for the improved tri-stable piezoelectric EH system, is solved by using the magnetizing current method [23]. As a result, taking this method into account, the magnetic force acting in the TPEH and ITPEH systems shown in Fig.3 being the simultaneous reaction of magnet A to a magnetic field produced by magnets located on the frame can be expressed in the following forms, respectively:

$$F_m = Fb_x + Fc_x = \mu_0 M_A S[(H_{yb2} - H_{yb1}) + (H_{yc2} - H_{yc1})] \tag{5a}$$

$$F_m = Fb_x + Fc_x + F_{Dx} =$$

$$\mu_0 M_A S \begin{bmatrix} (H_{yb2} - H_{yb1}) + \\ (H_{yc2} - H_{yc1}) + (H_{yD2} - H_{yD1}) \end{bmatrix} \tag{5b}$$

where: $\mu_0$ – the permeability of vacuum, $M_A$ - the magnitude of magnet's A magnetization, $S$ - the area of magnet's A the top or bottom surface, $H_{yb2}$, $H_{yb1}$ - the magnitudes of the magnetic field strength generated by the magnet $B$ at the centers of magnet A's top or bottom surfaces in $y$ direction, $H_{yc2}$, $H_{yc1}$ - the magnitudes of the magnetic field strength generated by the magnet $C$ at the centers of magnet A's top or bottom surfaces in $y$ direction, $H_{yD2}$, $H_{yD1}$ - the magnitudes of the magnetic field strength generated by the magnet $D$ at the centers of magnet A's top or bottom surfaces in $y$ direction.

While the field of the magnetic field strength according to [22] is expressed as:

$$H_{yb}(x,y,z) = \frac{M_B}{4\pi}\left( tan^{-1}\left(\frac{x_{B\_O1}z_{B\_O1}}{y\sqrt{x_{B\_O1}^2 + z_{B\_O1}^2 + y^2}}\right) + tan^{-1}\left(\frac{x_{B\_O2}z_{B\_O2}}{y\sqrt{x_{B\_O2}^2 + z_{B\_O2}^2 + y^2}}\right) \right.$$
$$\left. - tan^{-1}\left(\frac{x_{B\_O2}z_{B\_O1}}{y\sqrt{x_{B\_O2}^2 + z_{B\_O1}^2 + y^2}}\right) + tan^{-1}\left(\frac{x_{B\_O1}z_{B\_O2}}{y\sqrt{x_{B\_O1}^2 + z_{B\_O2}^2 + y^2}}\right) \right)$$

In addition, setting the center of magnets located on the frame as well as considering proper space coordinates of points O1 and O2 for particular magnets B, C and D are:

$$\left(x + \frac{h_A}{2}\cdot cos\,\varphi - \frac{x_1}{2}, x_2 - \frac{h_A}{2}\cdot sin\,\varphi, 0\right),$$
$$\left(x - \frac{h_A}{2}\cdot cos\,\varphi - \frac{x_1}{2}, x_2 - \frac{h_A}{2}\cdot sin\,\varphi, 0\right): \text{magnet B,}$$
$$\left(x + \frac{h_A}{2}\cdot cos\,\varphi + \frac{x_1}{2}, x_2 - \frac{h_A}{2}\cdot sin\,\varphi, 0\right),$$
$$\left(x - \frac{h_A}{2}\cdot cos\,\varphi + \frac{x_1}{2}, x_2 - \frac{h_A}{2}\cdot sin\,\varphi, 0\right): \text{magnet C,}$$
$$\left(x + \frac{h_A}{2}, x_2 - \frac{h_A}{2}, 0\right), \left(x - \frac{h_A}{2}, x_2 - \frac{h_A}{2}, 0\right): \text{magnet D}$$

can express the magnetic force given by Eq.(5a) for TPEH system and Eq.(5b) for ITPEH system in rewritten transformed form as:

$$F_m =$$
$$\mu_0 M_A S \begin{Bmatrix} H_{yb2}\left(x - \frac{h_A}{2}\cdot cos\,\varphi - \frac{x_1}{2}, x_2 - \frac{h_A}{2}\cdot sin\,\varphi, 0\right) \\ -H_{yb1}\left(x + \frac{h_A}{2}\cdot cos\,\varphi - \frac{x_1}{2}, x_2 - \frac{h_A}{2}\cdot sin\,\varphi, 0\right) \\ +H_{yc2}\left(x - \frac{h_A}{2}\cdot cos\,\varphi + \frac{x_1}{2}, x_2 - \frac{h_A}{2}\cdot sin\,\varphi, 0\right) \\ -H_{yc1}\left(x + \frac{h_A}{2}\cdot cos\,\varphi + \frac{x_1}{2}, x_2 - \frac{h_A}{2}\cdot sin\,\varphi, 0\right) \end{Bmatrix} \tag{6a}$$

$$F_m =$$
$$\mu_0 M_A S \begin{Bmatrix} H_{yb2}\left(x - \frac{h_A}{2}\cdot cos\,\varphi - \frac{x_1}{2}, x_2 - \frac{h_A}{2}\cdot sin\,\varphi, 0\right) \\ -H_{yb1}\left(x + \frac{h_A}{2}\cdot cos\,\varphi - \frac{x_1}{2}, x_2 - \frac{h_A}{2}\cdot sin\,\varphi, 0\right) \\ +H_{yc2}\left(x - \frac{h_A}{2}\cdot cos\,\varphi + \frac{x_1}{2}, x_2 - \frac{h_A}{2}\cdot sin\,\varphi, 0\right) \\ -H_{yc1}\left(x + \frac{h_A}{2}\cdot cos\,\varphi + \frac{x_1}{2}, x_2 - \frac{h_A}{2}\cdot sin\,\varphi, 0\right) \\ +H_{yD2}\left(x + \frac{h_A}{2}, x_2 + \frac{h_A}{2}, 0\right) \\ -H_{yD1}\left(x - \frac{h_A}{2}, x_2 - \frac{h_A}{2}, 0\right) \end{Bmatrix} \tag{6b}$$

The magnetic forces given by Eq.(6a) and Eq.(6b) lead to calculation the potential energies of TPEH and TPEH systems, including elastic potential energy and magnetic potential energy that can be written in the following forms:

$$U(x) = \frac{K_{ef}^2}{2}x^2 + \int F_m dx \tag{7}$$

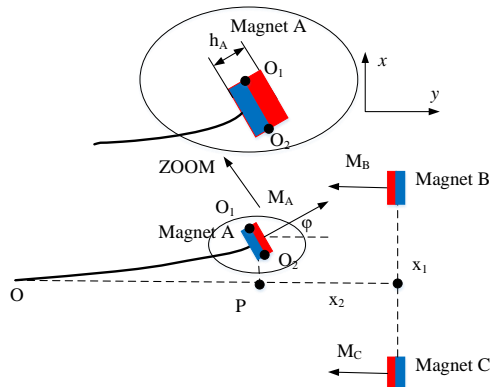where: $K_{ef}$ – the stiffness of the cantilever beam.

**Fig. 3.** Schematic of acting magnetic force in the TPEH system

## 4. NUMERICAL SIMULATIONS

In this section, the abilities of both tri-stable and improved tri-stable piezoelectric energy harvesting systems (TPEH and IT-PEH) under weak excitation were compared. To show the difference between them, simulations were conducted in Matlab and Ansys software by assuming that the magnetic moment of both external magnets ($mB=mC$=0.844 Am2) is twice higher than the magnetic moments of the tip magnet and the additional magnet ($mA=mD$=0.422 Am2). Moreover, to show how the additional magnet $D$ influences the behavior of the magnetic coupling system and the potential well depth, numerical calculations were performed for varying distance x1 between fixed magnets located on the frame, as well as varying air gaps x2 changing within the range of 11-13mm with a step of 1mm. The results of the potential energy calculated according to Eq.(7) are shown in Fig.4.
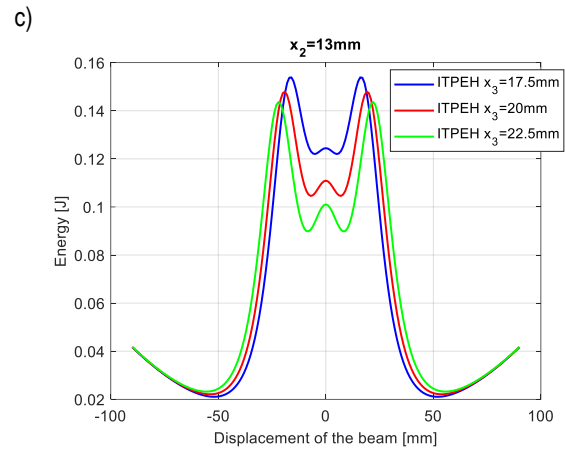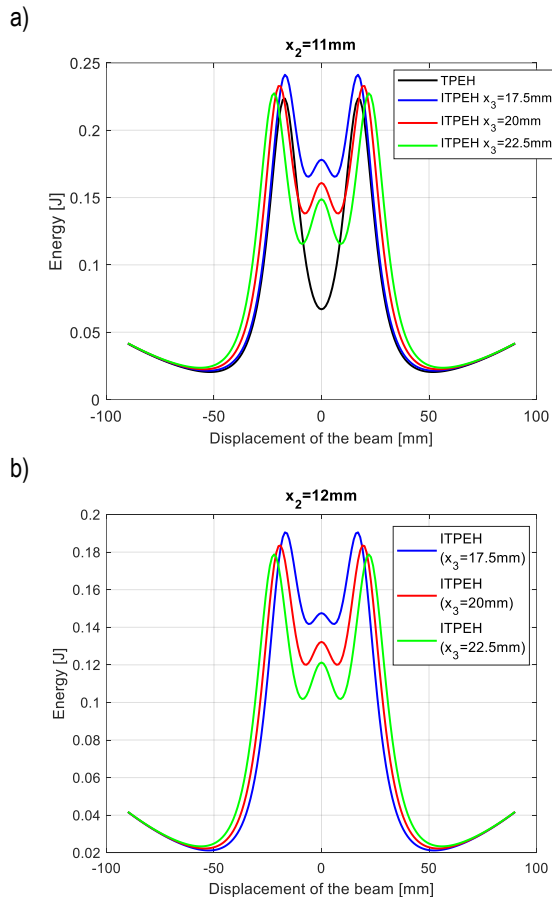
a)



b)



c)



**Fig. 4.** The comparison of the potential energy generated by the TPEH and ITPEH systems by various air gaps for distance between magnets a) x3=17.5mm, b) x3=20mm, c) x3=22.5mm

The analysis of the potential energy in both EH systems indicated a significant influence of additional magnets on the behavior of the improved tri-stable systems. Compared to the TPEH, in the ITPEH system, the depth of the middle potential wells decreases by reducing the air gaps between the tip magnet and the additional magnet. Further analysis allows us to also observe that extending the distance between fixed magnets leads to a higher effect of additional magnets on the vibrating structure, especially in the neutral position of the vibrating beam, as well as to deepening potential barriers. As a result, such behavior of the proposed system leads to the conclusion that the most enhanced broadband energy harvesting effect for all considered air gaps is achieved for the ITPEH system with an air gap of 11mm, as well as by the highest distance between magnets of x3=22.5mm, while the lowest broadband effect [25-27] for the same EH system but with a distance of x3=17.5mm.

In the next step, the behavior of the tri-stable and improved tri-stable energy harvesting systems was analyzed in the time domain by using Matlab software. In order to do this, firstly coefficients of the magnetic force given by Eq.(2) were determined by using the curve fitting method, and next Eq.(3) whereby using Runge-Kutta algorithm values of displacement and voltage generated by the piezo-elements in the time domain are calculated. Simulations were performed for both considered EH systems with three various air gaps between the tip magnet and the fixed magnet (x2=11,12,13mm), as well as three different distances between magnets x3 which equaled 35mm, 40mm, and 45mm, respectively. In addition, these simulations were also performed for three different base accelerations 0,91g, 1,34g, and 1,73g, respectively. Chosen results are presented in Fig.5, while their deeper analysis versus experimental results is described in the next Section.

The analysis of the voltage signals generated by the piezo-elements in the tri-stable energy harvesting system indicated a significant increase in their values, especially within the range marked by a rectangle with dash line where the influence of the magnetic force on the vibrating structure is higher. As a result, the effectiveness of the improved tri-stable EH system for all considered cases is improved and enhanced.

The last step of numerical simulations was related to comparing the power output generated by the conventional tri-stable energy harvesting system, the improved tri-stable energy harvesting system and bi-stable energy harvesting system where the

Andrzej Koszewnik, Bartłomiej Ambrożkiewicz
*Enhanced Broadband Tri-Stable Energy Harvesting System by Adapting Potential Energy – Experimental Study*

DOI 10.2478/ama-2024-0066

same type of the beam, piezo-harvester and magnets were used. In order to do this, the clearance between the tip magnet located on the beam and the fixed magnet x2 was set at 11mm, while distance x1 for the TPEH system was set at 45mm, as well as distance x3 for the ITPEH system was set at 22.5mm. In addition, considering the above parameters, simulations were performed for an impedance load close to the quasi-optimal value (Ropt=1.5MΩ), changing within the range of 1.1MΩ - 2.1MΩ. The calculated values of the power outputs generated from mathematical models of particular EH systems are presented in Fig.6.

The analysis of the power output generated by each EH system shows that the highest power output (over 80mW) is obtained for the improved tri-stable energy harvesting system connected with the quasi-optimal impedance load, while the lowest output – for the bi-stable energy harvesting system. Such behavior of these systems is due to the considered additional magnet in the system that leads to a stronger impact of the nonlinear magnetic force to the vibrating structure, and to improving the effectiveness of the system.
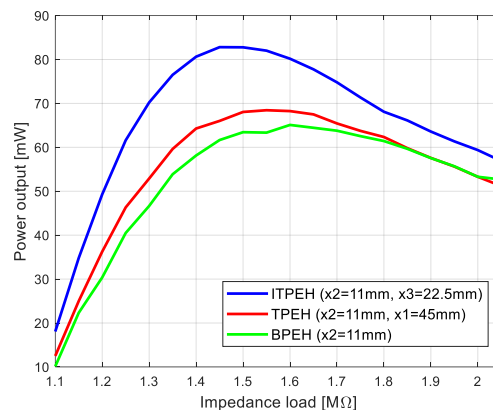
a)



b)



**Fig. 5.** The comparison of voltage generated by the piezo-element located on the beam excited to vibration with base acceleration increasing up to 1.73g from a) the conventional tri-stable EH system b) the improved tri-stable energy harvesting system



**Fig. 6.** The comparison of the power output generated by the improved tri-stable EH system, conventional tri-stable EH system and bi-stable EH system by various impedance load connected to the piezo-sensor

## 5. EXPERIMENTAL INVESTIGATIONS

In this section, the process of assessment parameters of both TPEH and ITPEH systems is carried out on the lab stand shown in Fig.7. In order to do this, the fiberglass beam, which represents a host structure, is equipped in a piezo patch composite of type 8514 P2, and it is located 10mm from the fixed end of the beam and the neodymium magnet N35 of type MP 14/4 x 3 placed close to the free end of the same beam, respectively. The parameters of the beam, piezo harvester, and neodymium magnets are collected in Tab.1. Apart from the aforementioned elements, the lab stand is also equipped with a frame where the appropriate amount of neodymium magnets is placed. To perform experimental tests of the tri-stable EH system, two neodymium magnets with the same magnetic moments were located symmetrically versus the beam on the frame. In contrast, in the case of the improved tri-stable energy harvesting system – the lab stand was filled with additional neodymium with the twice lower magnetic moment that was located on the frame in the middle of the external magnets. Additionally, the laboratory stand was retrofitted into two other devices: the signal generator Agilent and the vibration shaker TV51110M with a BAA 120 amplifier, that were used to generate signal excitation and apply it to the vibrating structure. Whereas, from the measurement point of view, the lab stand was equipped with a data acquisition system (DAQ) with a measurement card of type USB-6341, the displacement sensor LG10A65PUQ and the 3-axis accelerometer that is used to measure the voltage generated by the piezo, deflection of the tip mass of the beam, and base acceleration, respectively.
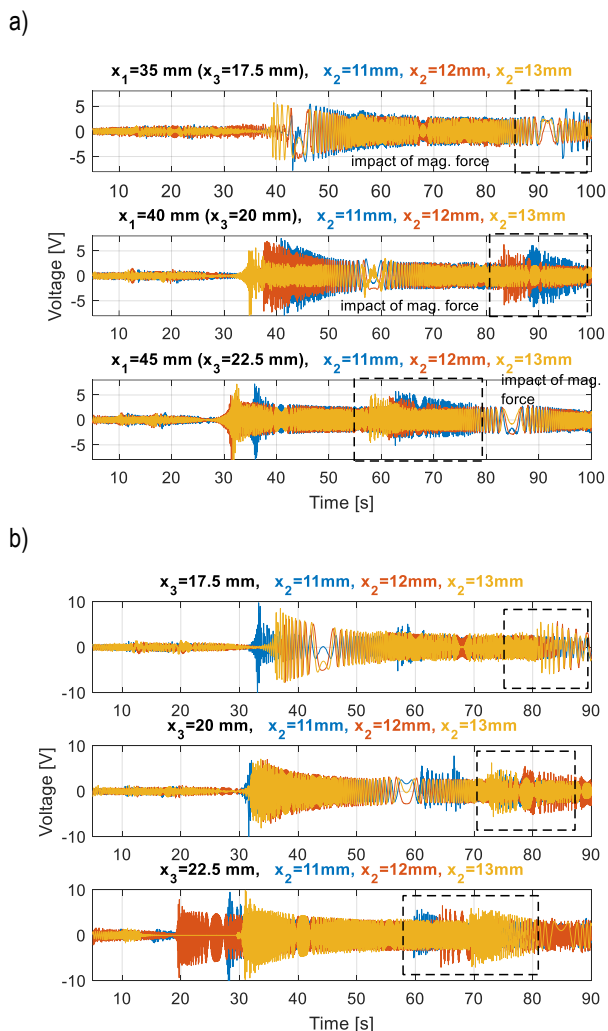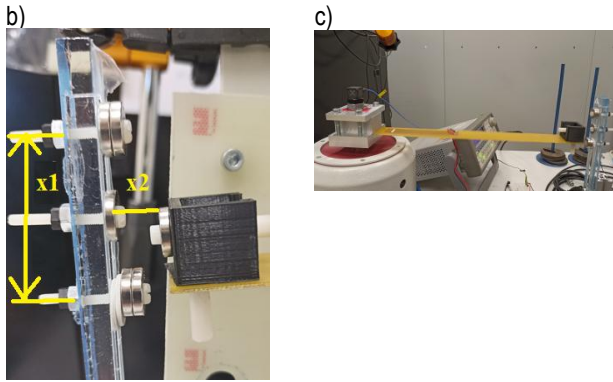
a)

**Fig. 7.** The photo of the lab stand a) the whole lab stand, b) the view of the frame with three neodymium magnets for testing the ITPEH system, c) the view of the piezoelectric cantilever beam during the test

**Tab.1.** Parameters of the cantilever beam, piezo patch composites MFC8514 and neodymium magnets

| Mechanical Parameters | | | | | | |
|---|---|---|---|---|---|---|
| *Fiber Glass* | | | | | | |
| Length [mm] | Width [mm] | Length [mm] | | | | |
| $L_F$  270 | $w_F$  38 | $t_F$  1.5 | | | | |
| Young's Modulus (GPa) | Poisson's Ratio (-) | Density [kg/m3] | | | | |
| $E_F$  80 | $v_F$  0.22 | $\rho_F$ 2600 | | | | |
| | | | | | | |
| *Piezo composite MFC* | | | | | | |
| Young's Modulus (GPa) | Poisson's Ratio (-) | | Piezo. Charge Coeff. (pC/N) | Relative Permittivity (-) | | |
| | | | | | | |
| $E_x$ 31.6 | $v_{xy}$  0.4 | | $d_{31}$ −173 | $\varepsilon_r^T$  2253 | | |
| $E_y$ 17.1 | $v_{yz}$  0.2 | | $d_{32}$ −150 | | | |
| $E_z$ 9.5 | $v_{xz}$  0.4 | | $d_{33}$ 325 | | | |
| Geometrical parameters | | | | | | |
| Overall Length [mm] | Overall Width [mm] | Active Length [mm] | Active Width [mm] | Thick. of PZT fiber layer [µm] | Thick. of electrode layer [µm] | Thick. of Caption layer [µm] |
| $L_p$  103 | $w_P$  17 | 85 | 14 | 180 | 25 | 30 |
| | | | | | | |
| *Neodymium magnet N35 – tip magnet A and internal D* | | | | | | |
| Outer/Inner diameter [mm] | Thickness [mm] | | Strength [kg] | | Remanence [T] | |
| 14/4 | 3 | | 2.5 | | 1.2 | |
| *Neodymium magnet N35 – external magnet B and C* | | | | | | |
| 14/4 | 5 | | 5.0 | | 1.21 | |

In the first step, the experimental tests were focused on assessing the value of the base acceleration by various values of the chirp signal amplitude. To do this, an excitation signal with three different amplitudes in the range of 3-5V with a step of 1V by linearly increasing frequency from 1Hz to 40Hz in the period of 120s was firstly generated by the signal generator and next applied to the vibration shaker. Then, the 3-axis accelerometer placed directly on the vibration shaker-base with a sensitivity of 104.5mV/g in the vertical axis allowed the assessment of maximum values of the base acceleration 0.91g, 1.34g, and 1.73g, corresponding to the amplitude of the excitation signal 3V, 4V, 5V, by the frequency of 40Hz, respectively.

Next, the behavior of both tri-stable and improved tri-stable energy harvesting systems were compared on the lab stand in the time domain. To do this, all tests were conducted for three different air gaps $x2$ changing in the range of 11-13 mm. Moreover, in the case of the tri-stable piezoelectric energy harvesting system, the experimental tests were carried out for three different distances $x1$ between the fixed magnets $B$ and $C$ in the range of 35-45mm with a step of 5mm. While in the case of the improved tri-stable system - by three different distances $x3$ between chosen external fixed magnet $B$ and additional magnet $D$ in the range of 17.5-22.5mm with a step of 2.5mm. As a result, it led to the conduct of nine different tests for two separate EH systems by various base accelerations where the AC voltage output from the piezo was measured and recorded for each try. Finally, the results obtained from testing the TPEH system are shown in Fig.8, while from testing the ITPEH system - in Fig.9.

The conducted analysis of the recorded signals shown in Fig.8 for the TPEH system with the narrowest distance between the magnet, as well as the smallest air gap of 11mm indicated a light increase of the voltage output from the piezo only to 3.47V, that is due to a weak impact of the nonlinear magnetic force on the vibrating beam. Other results can be observed for the EH system with magnets spaced 40mm apart and excited to vibration with a lightly higher base acceleration (0.91g) – see Fig.8b. Then, increasing the base acceleration to 1.34g and expanding distance $x1$ between magnets leads to increasing the impact of the magnetic force on the structure for all considered air gaps and generating higher voltages than previously. In addition, it can be observed that the widening of the air gap leads to a decreasing amplitude of the magnetic force and consequently to its faster appearance in the magnetic coupling EH system. Yet another behavior can be shown in Fig.8c for the fixed magnets spaced 45 mm apart. Then, the base acceleration equals 1.73g by a frequency of 40Hz leading to an enhanced impact of the magnetic force to the system and appearing additional vibrations with an amplitude of over 5V in a transient period of 55-80s.

Next, the analysis was performed for the ITPEH system. Taking into account the diagrams presented in Fig.9, it can be seen that the considered additional magnet, in the TPEH system, allows for improvement of the behavior of the coupling magnetic EH system. It is especially shown by the configuration of the ITPEH system with the narrowest distance between magnets, as well as the smallest air gap, where the testing system generates higher voltage output (by 0.8V) than the TPEH system at the same base acceleration. Similar results can be observed in Fig.9b and Fig.9c, where the ITPEH system leads to obtaining the voltage output higher by 1.2V at the same initial conditions (distance between magnets equals 17.5mm and air-gap equals 11mm) . As a result, it allows us to conclude that adapting the potential energy of the EH system by considering additional magnets in the coupling magnetic EH system leads to generating higher voltages and, finally, to improve the effectiveness of the proposed ITPEH system.

Andrzej Koszewnik, Bartłomiej Ambrożkiewicz
*Enhanced Broadband Tri-Stable Energy Harvesting System  by Adapting Potential Energy – Experimental Study*

DOI 10.2478/ama-2024-0066

To confirm the above results, as well as show how nonlinear magnetic force affects the beam structure, a deeper analysis of the recorded voltage output signals was performed in chosen periods of time marked in Fig.8 and Fig.9, where increasing voltage amplitudes can be observed. The obtained results  are presented in Fig.10-Fig.12 separately for three different distances between  magnets *x3* where voltage output generated by both TPEH and IPTEH systems were compared.
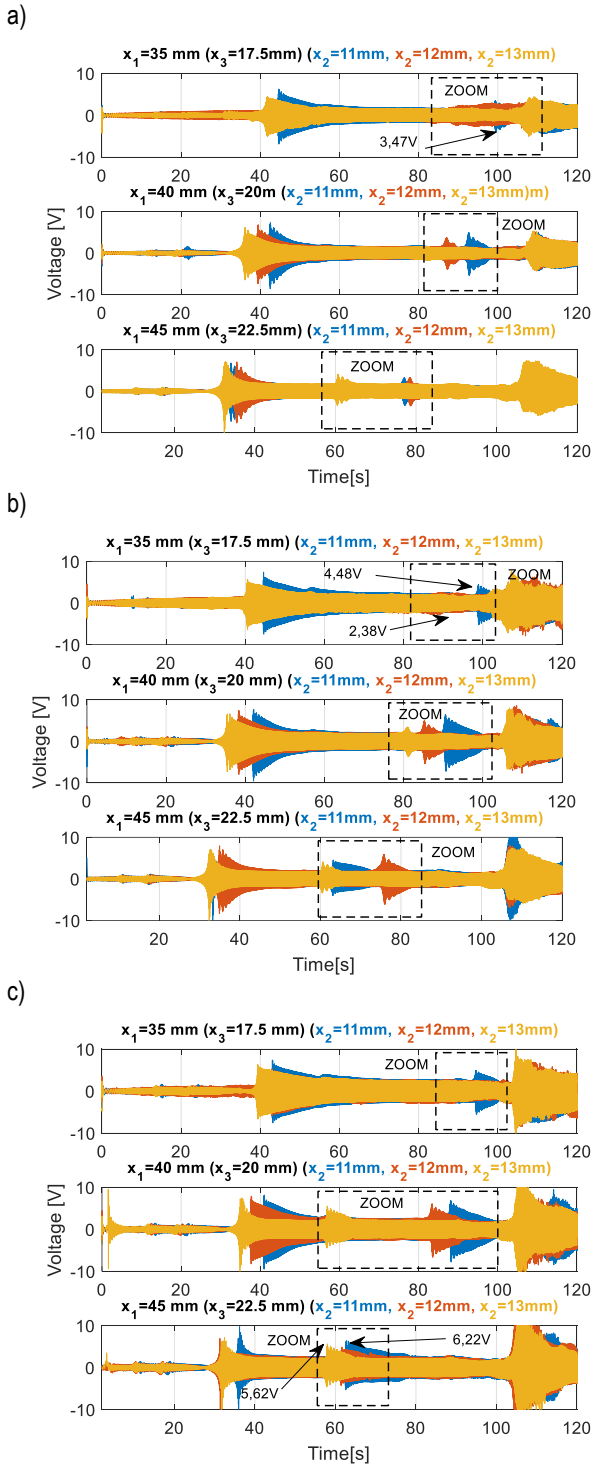


**Fig. 8.** The comparison of the voltage output from the piezo for the TPEH system by various air gaps in the range of 11-13mm and the distance between fixed magnets for a) increasing of the base acceleration to 0.91g, b) increasing the base acceleration to 1.34g, c) increasing the base acceleration to 1.73g



**Fig. 9.** The comparison of the voltage output from the piezo for the ITPEH system by various air gaps in the range of 11-13mm and the distance between fixed magnets for a) increasing the base acceleration to 0.91g, b) increasing the base acceleration to 1.34g, c) increasing the base acceleration to 1.73g
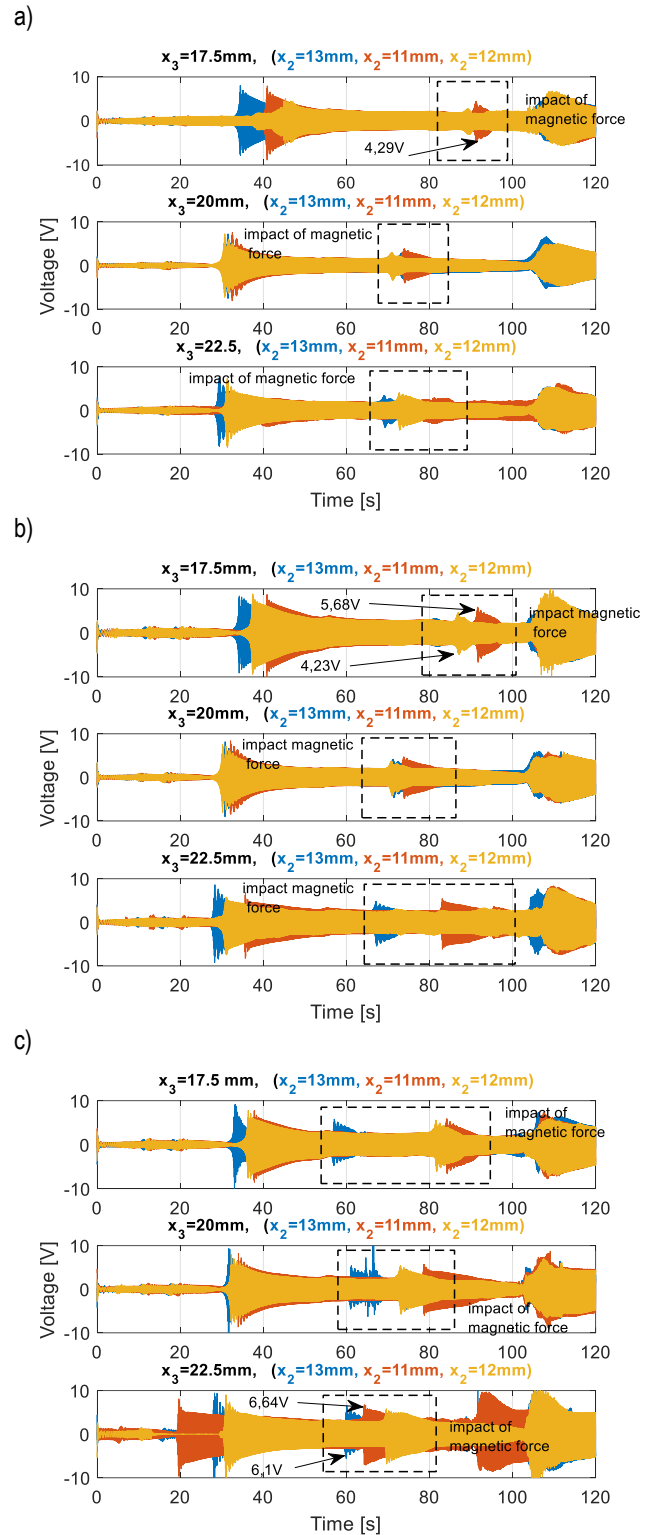
The analysis of these voltage outputs generated by both systems indicated the advantage of the ITPEH system over the TPEH system for each configuration of the magnetic coupled EH system. It is especially visible in Fig.9 where the adapting the potential energy by setting the narrowest distance between the magnets,

air gaps equal 12mm or 13mm, and the amplitude of the base acceleration over 0.91g leads to the appearance of the magnetic force with low amplitude only for the ITPEH system. Another behavior can be observed for both tri-stable systems working with an air gap of 13mm where a weak base excitation leads to the disappearing impact of the magnetic force on the structure. This behavior is caused by a deep middle potential well. Further analysis of diagrams presented in Fig.10 also shows that the ITPEH system works with the narrowest air gap, which equals 11 mm, as well as with the narrowest distance between magnets allowing to better strengthen the impact of the magnetic force on the vibrating structure.
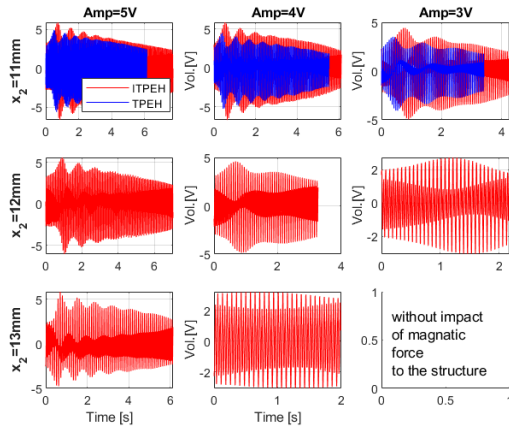
voltage signals presented in Figs.10-12 (see Tab.2) are a confirmation of the obtained results. The analysis of these values indicated the advantage of the ITPEH system over the TPEH system by obtaining higher values for ITPEH system versus TPEH system each time. As a result, again the highest value was obtained for the system which operates with the distance between magnets of 22.5mm, the narrowest air gap of 11mm, while the lowest - for the system with the smallest distance x3=17.5mm. Thus, taking the obtained results into account, it can be concluded that adapting the potential energy in the tri-stable energy harvesting system under weak excitation leads to increase.



**Fig. 10.** The comparison of the recorded voltage output signals generated by the TPEH and ITPEH systems in the indicated time period of impacting the magnetic force on the structure by the distance between fixed magnets x3=17.5 mm
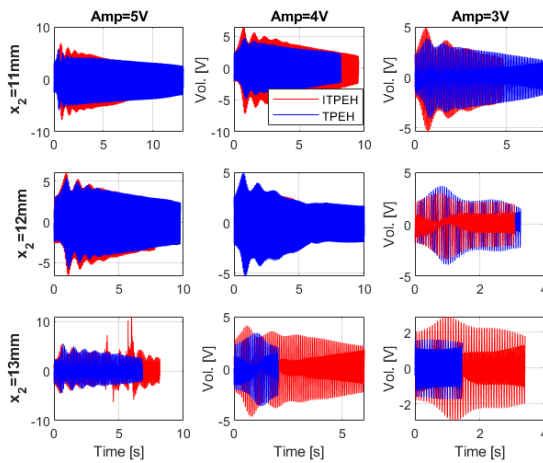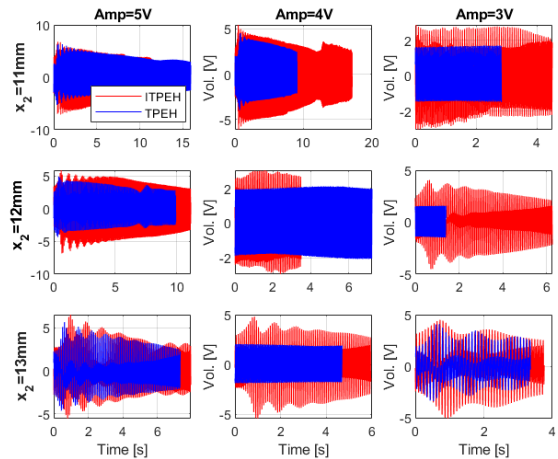


**Fig. 12.** The comparison of the recorded voltage output signals generated by the TPEH and ITPEH systems in the indicated time period of impacting the magnetic force on the structure by the distance between fixed magnets x3=22.5 mm

**Tab. 2.** The calculated RMS values of the recorded voltage signals for TPEH and ITPEH systems (maximal RMS values in each configuration are marked with red font)

| The base acceleration from 0 to 0.91g (40Hz) | | | |
|---|---|---|---|
| air gap $x_2$ [mm] | Distance between fixed magnets $x_3$ [mm] | | |
| | 17.5mm | 20mm | 22.5mm |
| | TPEH / ITPEH | | |
| 11mm | 1.5820 / 1.8829 | 1.5187 / 1.8304 | 1.0563 / 1.4286 |
| 12mm | - / 1.4406 | 1.3542 / 1.5293 | 0.9896 / 1.6852 |
| 13mm | -/ - | 0.9394 / 1.2979 | 1.5469 / 1.5274 |
| | | | |
| **The base acceleration from 0 to 1.34g (40Hz)** | | | |
| air gap $x_2$ [mm] | Distance between fixed magnets $x_3$ [mm] | | |
| | 17.5mm | 20mm | 22.5mm |
| | TPEH / ITPEH | | |
| 11mm | 1.9211 / 2.3739 | 1.8531 / 2.3609 | 1.7419 / 2.0847 |
| 12mm | -/ 2.0586 | 1.6343/ 1.6395 | 1.3076 / 1.6832 |
| 13mm | - / 1.7698 | 1.5996/ 1.7405 | 1.3097 / 2.0513 |
| | | | |
| **The base acceleration from 0 to 1.73g (40Hz)** | | | |
| air gap $x_2$ [mm] | Distance between fixed magnets $x_3$ [mm] | | |
| | 17.5mm | 20mm | 22.5mm |
| | **TPEH / ITPEH** | | |
| 11mm | 2.1309/ 2.3189 | **2.2014 / 2.3609** | **2.1714 / 2.7127** |
| 12mm | -/ 2.1607 | **1.6343/ 2.1017** | **1.9120 / 2.4722** |
| 13mm | -./ 2.0208 | 1.5996/ 2.1633 | 1.8998 / 2.1865 |



**Fig. 11.** The comparison of the recorded voltage output signals generated by the TPEH and ITPEH systems in the indicated time period of impacting the magnetic force on the structure by the distance between fixed magnets x3=20 mm

As a result, the piezo sensor attached to the beam generates a higher amplitude of voltage in a longer time. Similar results can be observed in diagrams presented in Fig.11 and Fig.12 for both EH systems working with two different distances between magnets (*x3*=20mm and *x3*=22.5mm), where considering an additional magnet in the TPEH system allowed to strengthen the impact of the nonlinear magnetic force on the structure and, consequently, to generate voltages with higher amplitudes by the piezo element. Additionally, the RMS values calculated for the total length of

Andrzej Koszewnik, Bartłomiej Ambrożkiewicz
*Enhanced Broadband Tri-Stable Energy Harvesting System by Adapting Potential Energy – Experimental Study*

DOI 10.2478/ama-2024-0066

The obtained results and RMS values were verified additionally by performing the time-frequency analysis of TPEH and ITPEH systems. In order to do this, the continuous wavelet transform method based on analytical Morse wavelet [35,36] was used for the voltage output signals generated by the piezo and systems excited to vibration with the highest considered base acceleration.
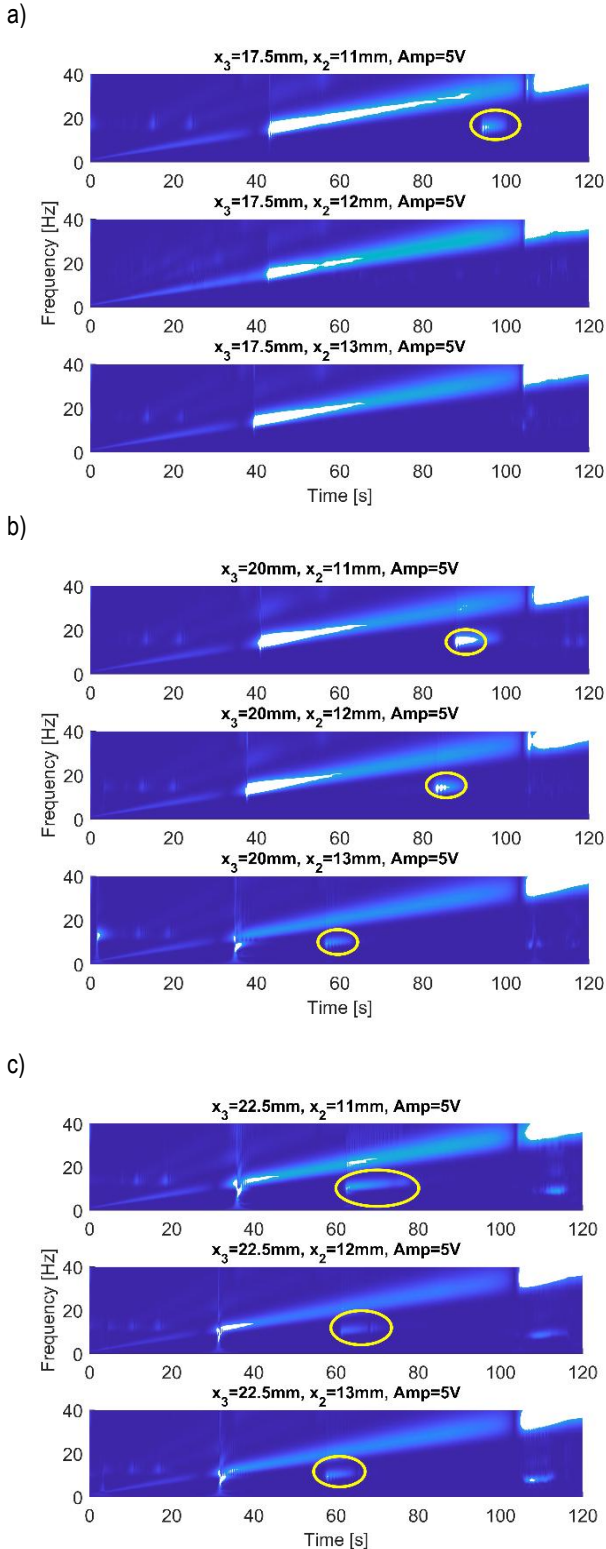


**Fig. 13.** The comparison of time-frequency plots of the TPEH system excited to vibration with base acceleration of 1.73g by various air gaps and distance between fixed magnets



**Fig. 14.** The comparison of time-frequency plots of the ITPEH system excited to vibration with base acceleration of 1.73g by various air gaps and distance between fixed magnets
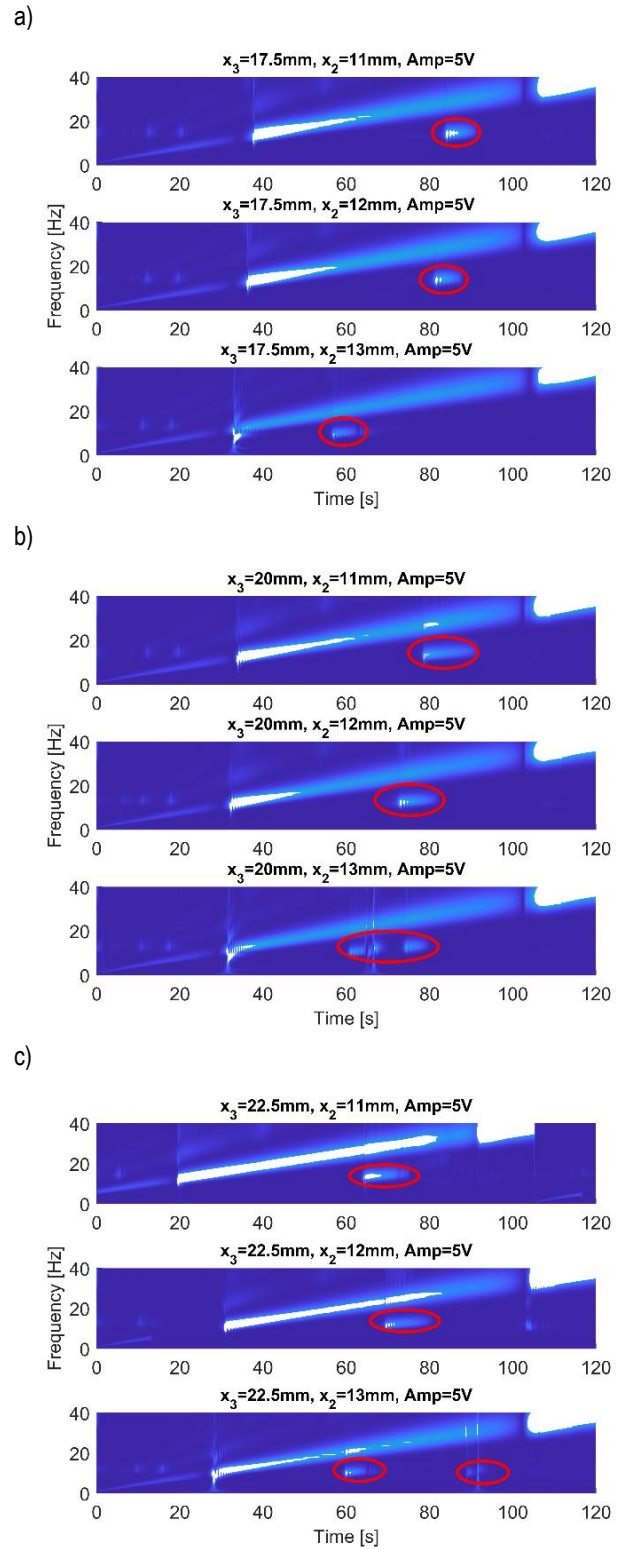
The analysis of diagrams shown in Fig.13 and Fig.14 indicated once more that the width of the air gap by assuming other parameters of conventional and the improved tri-stable systems, like distance between magnets x3 and base acceleration, as constant, significantly influence appearing the magnetic force in these systems and, consequently, their behavior. Taking this into

account, nonlinear magnetic force appeared only in the TPEH system working with the narrowest air gap, and excited to vibration with a frequency in the range of 25-29Hz. Further analysis of diagrams presented in Fig.13b shows that the gradual increase of the air gap by widenning the distance between the fixed magnets to 40mm leads to the appearance of the magnetic force in a lower range of frequency excitation than it was previously. Similar results were achieved by further expanding the distance between the magnets to 45mm. Then, a gradual increase of clearance between the tip magnet and the fixed magnets leads to a shortened transient period affecting the magnetic force to the structure. As a result, the strongest vibration-based energy harvesting effect is achieved during the analysis of the TPEH system with an air gap of 11mm and the widest distance between fixed magnets (6.22V), while the lowest (5,62V) by the air gap of 13mm.

Further analysis of the time-frequency diagrams determined for the ITPEH system proved again that considering of an additional fixed neodymium magnet, located on the frame, allowed for an improved energy harvesting effect. It is especially observable in diagrams in Fig.14c for the system with an air gap of 11mm, where the transient period of impacting of the magnetic force to the structure is longer and their amplitude is higher in comparison to the TPEH system (see Fig.13c). Similar result was achieved for other ITPEH system activities with the air gap of over 11mm, where impacting of the magnetic force was also higher than in the case of the TPEH system working in the same conditional parameters.

The last step of this subsection is verification of the simulated results. In order to do this, all experimental and simulation results obtained by three various base accelerations, as well as considered different distances of x1, x2 and x3, are collected in Tabs .3-5.

**Tab. 3.** The comparison of the voltage generated by the piezo (simulation and experimental results) by the base acceleration increasing up to 0.91g

| Base acceleration 0.91g (TPEH) | | | | | | | | |
|---|---|---|---|---|---|---|---|---|
| **x1 [mm]** | Simulation | | | Experiment | | | Error | | |
| | air gap x2 [mm] | | | air gap x2 [mm] | | | air gap x2 [mm] | | |
| | 11 | 12 | 13 | 11 | 12 | 13 | 11 | 12 | 13 |
| 35mm | 4,73 | - | - | 4,6 | - | - | 0,17 | - | - |
| 40mm | 6,75 | | - | 6,04 | 5,66 | | 0,71 | 0,34 | - |
| 45m | 6,06 | 4,76 | 4,40 | 5,5 | 4,25 | 4,15 | 0,56 | 0,15 | 0,25 |
| **Base acceleration 0.91g (ITPEH)** | | | | | | | | | |
| **x3 [mm** | Simulation | | | Experiment | | | Error | | |
| | air gap x2 [mm] | | | air gap x2 [mm] | | | air gap x2 [mm] | | |
| | 11 | 12 | 13 | 11 | 12 | 13 | 11 | 12 | 13 |
| 17.5mm | - | 4,43 | 2,70 | - | 3,87 | 2,43 | - | 0,56 | 0,29 |
| 20mm | 4,20V | 3.05 | 2,70 | 3,82 | 2,86 | 2,53 | 0,38 | 0,19 | 0,17 |
| 22.5mm | 3,41V | 4,2 | 3,64 | 3.1 | 4 | 3,45 | 0,31 | 0,2 | 0,19 |

**Tab. 4.** The comparison of the voltage generated by the piezo (simulation and experimental results) by the base acceleration increasing up to 1.34g

| Base acceleration 1.34g (TPEH) | | | | | | | | |
|---|---|---|---|---|---|---|---|---|
| **x1 [mm]** | Simulation | | | Experiment | | | Error | | |
| | air gap x2 [mm] | | | air gap x2 [mm] | | | air gap x2 [mm] | | |
| | 11 | 12 | 13 | 11 | 12 | 13 | 11 | 12 | 13 |
| 35mm | 4,05 | - | - | 3.79 | - | - | 0,26 | - | - |
| 40mm | 6,55 | 4,85 | 3.1 | 6.31 | 4,54 | 3,30 | 0,24 | 0,31 | 0,2 |
| 45mm | 3,9 | 5,71 | 2,86 | 3,7 | 5,6 | 3,25 | 0,2 | 0,11 | 0,39 |
| **Base acceleration 1.34g (ITPEH)** | | | | | | | | | |
| **X3 [mm]** | Simulation | | | Experiment | | | Error | | |
| | air gap x2 [mm] | | | air gap x2 [mm] | | | air gap x2 [mm] | | |
| | 11 | 12 | 13 | 11 | 12 | 13 | 11 | 12 | 13 |
| 17.5mm | 6,24 | 4,44 | 3,69 | 5,68 | 4,23 | 3,21 | 0,56 | 0,19 | 0,48 |
| 20mm | 4,36 | 3,81 | 4,37 | 4,16 | 3,63 | 3,8 | 0,20 | 0,18 | 0,57 |
| 22.5m | 5,14 | 4,93 | 4,85 | 4,9 | 4,7 | 4,42 | 0,24 | 0,23 | 0,43 |

**Tab. 5.** The comparison of the voltage generated by the piezo (simulation and experimental results) by the base acceleration increasing up to 1.73g

| Base acceleration 1.73g (TPEH) | | | | | | | | |
|---|---|---|---|---|---|---|---|---|
| **x1 [mm]** | Simulation | | | Experiment | | | Error | | |
| | air gap x2 [mm] | | | air gap x2 [mm] | | | air gap x2 [mm] | | |
| | 11 | 12 | 13 | 11 | 12 | 13 | 11 | 12 | 13 |
| 35mm | 3,55 | - | - | 3,22 | - | - | 0,33 | - | - |
| 40mm | 5,15 | 3,97 | - | 4,8 | 3,68 | - | 0.35 | | - |
| 45mm | 3,72 | 3,42 | 3,47 | 3,5 | 3,2 | 3,04 | 0,22 | 0,22 | 0,43 |
| **Base acceleration 1.73g (ITPEH)** | | | | | | | | | |
| **x3 [mm]** | Simulation | | | Experiment | | | Error | | |
| | air gap x2 [mm] | | | air gap x2 [mm] | | | air gap x2 [mm] | | |
| | 11 | 12 | 13 | 11 | 12 | 13 | 11 | 12 | 13 |
| 17.5mm | 5,5 | 5,2 | 5,3 | 5,22 | 5,42 | 5,4 | 0,23 | 0,22 | 0,1 |
| 20mm | 5,8 | 5,4 | 5,72 | 5,69 | 5,34 | 5,42 | 0,11 | 0,06 | 0,3 |
| 22.5mm | 6,74 | 5,53 | 5,87 | 6,54 | 5,41 | 6,1 | 0,20 | 0,12 | 0,23 |

Taking into account the values of voltage collected in the Tab.3-Tab.5, it can be noticed that the experimental results

properly verified the amplitudes calculated in the numerical way in all considered cases. Their further analysis indicates that the amplitude of voltage generated by the real piezo-composite is lightly lower than those calculated on the basis of the mathematical model. This behavior is due to a lower amplitude of the magnetic force which affects the structure to vibrating, as well as heterogeneity of the adhesive layer between the MFC element and the host structure.

## 6. THE ANALYSIS OF PHASE PORTRAITS OF TPEH AND ITPEH SYSTEMS

The last step of the experimental test was related to determining the portrait phases of both TPEH and ITPEH systems by considering the repulsion effect of the magnetic force. To do this, tests were carried out for chirp signal with frequency increasing from 1Hz to 40Hz, and by three different amplitudes where displacement of the tip mass was measured by using the laser displacement sensor placed 75mm from the vibrating structure for each time. Similarly, as it was previously, tests were carried out for three different distances between magnets $x3$ as well as three various air gaps $x2$ in the range of 11-13mm. As a result, nine different tests were conducted for each system, where the most interesting ones are presented in Figs.15-17.
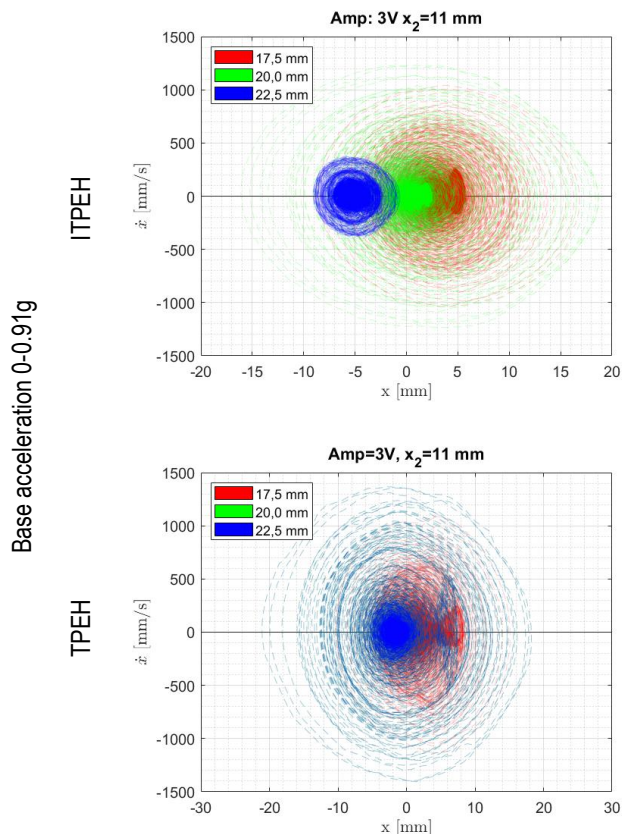


**Fig. 15.** The comparison phase portrait of both TPEH and ITPEH systems by various air gaps in the range of 11-13mm and increasing base acceleration from 0 to 0.91g
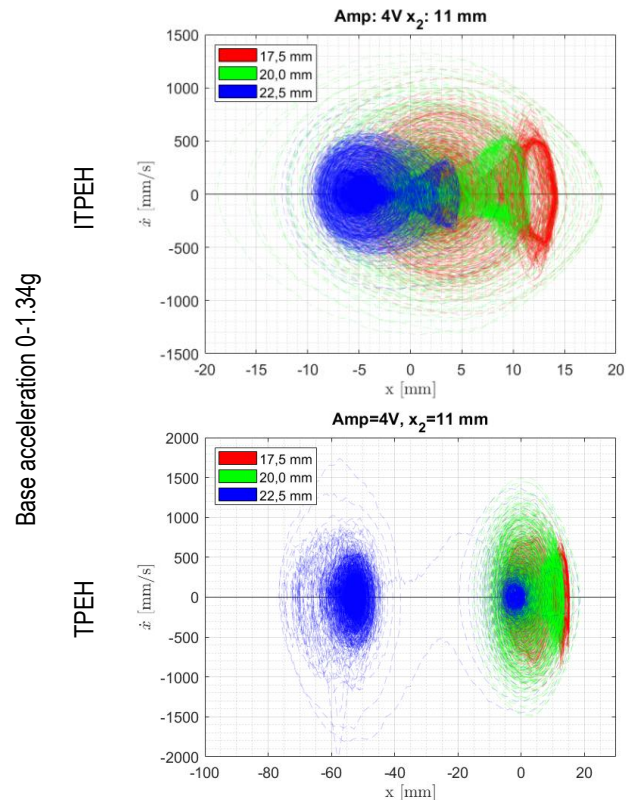


**Fig. 16.** The comparison phase portrait of both TPEH and ITPEH systems by various air gaps in the range of 11-13mm and increasing base acceleration from 0 to 1.34g



**Fig. 17.** The comparison phase portrait of both TPEH and ITPEH systems by various air gaps in the range of 11-13mm and increasing base acceleration from 0 to 1.73g
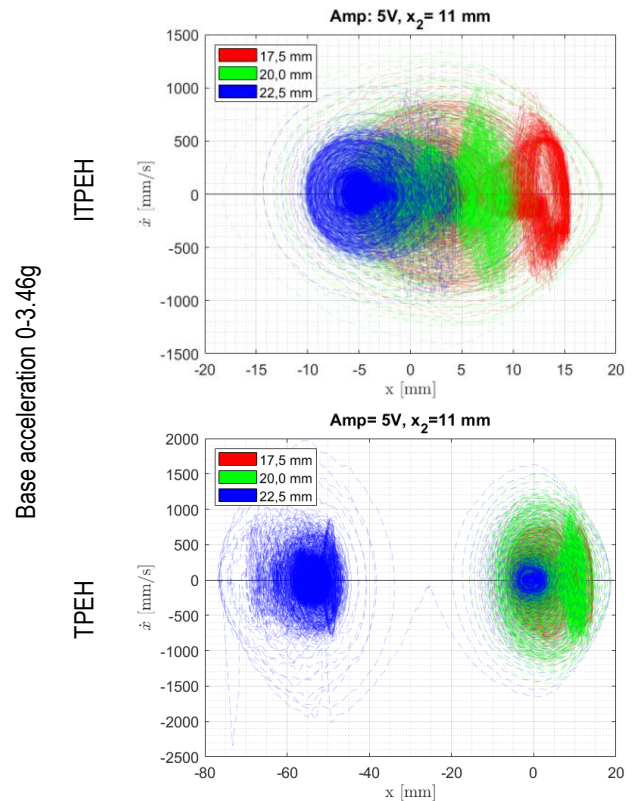
Observing diagrams presented in Fig.15b indicated that low amplitude base acceleration leads to generating three different trajectories of phase portrait of TPEH systems concentrated around the singular equilibrium point. This behavior is due to a weak impact of the magnetic force on the structure, which is also a result of the existent deep middle potential well and high potential barriers. Slightly different behavior can be observed during the analysis of particular portrait phases generated by the improved tri-stable energy harvesting system. Then, the low value of base acceleration and reduced distance between the additional magnet and the external magnets again leads to appearing weak magnetic force and generating small elliptical trajectories in the diagram.

Next, the analysis of portrait phases in Fig.16b shows that a slightly increase of base acceleration and the choice of an appropriate distance between the fixed magnets can significantly affect the behavior of the TPEH system. It is especially shown that the TPEH system works with the highest distance between magnets $x3$ of 45mm, where increasing the frequency excitation leads to appearing a higher amplitude of the beam vibration and consequently jumping of EH system to the bottom potential wall. A completely other behavior can be shown during the analysis of the ITPEH system (see Fig.15a) where tailoring potential energy caused by considering additional fixed magnets leads to increasing the magnetic field in the coupling system and generates a conical nature of particular portrait phases. As a result, the highest elliptical trajectories are generated for the system with the narrowest spacing between magnets ($x3$=17.5mm), while the lowest one - for the system with the widest spacing ($x3$=22.5mm). Slightly different results can be observed during the analysis of both TPEH and ITPEH systems excited to vibration with the highest amplitude of acceleration. Then, strong nonlinearity in the improved tri-stable EH systems leads to increased velocity of vibrations and jumping the vibrating beam between potential wells in all considered configurations.

## 7. SUMMARY AND CONCLUSIONS

The broadband effect of the tri-stable and improved tri-stable energy harvesting systems by various air gaps as well as distances between fixed magnets under weak excitation was analyzed in this paper. To do this, firstly the model of magnetic coupling energy harvesting systems was determined, where nonlinear magnetic force existing in the model was calculated by using the magnetization current method. Next, numerical simulations of the conventional tri-stable and the improved EH systems were performed by using Matlab software. The obtained diagrams of potential energies of both systems by various air gaps changing in the range of 11-13mm and different distances between fixed magnets indicated shallowing of the depth of the middle potential well with a decrease of the air gap and consequently improved behavior of the proposed tri-stable energy harvesting system. In addition, it can be observed that extending the distance $x3$ between the fixed magnets leads to a higher effect of an additional magnet in the ITPEH system to vibrating beam as well as deepening of potential barriers. Finally, taking these results into account, the energy harvesting effect was most enhanced for the ITPEH system activities by the narrowest air gap ($x2$=11mm) and the distance between the magnets ($x3$=22.5), while the lowest - for the system activities in configuration $x2$=11mm and $x3$=17.5mm.

The experimental tests of the TPEH and ITPEH systems car-

ried out on the lab stand for both real structures properly verified the numerical calculations. Comparing the results of the voltage output from the piezo-sensor again proved that the most impact of nonlinear magnetic force on the vibrating structure is achieved for the improved tri-stable energy harvesting system working with the narrowest air gap and the largest distance between the fixed magnets. The diagrams presented in Figs. 8-10 confirm these results. Their analysis indicated that introducing a singular additional fixed magnet to the conventional TPEH behavior of a magnetic coupling EH system can be increased. Especially, it can be seen in Fig.8 where a low value of base acceleration allows the magnetic force to appear in both systems only by air gap which equal 11mm. In the case of other air gaps, nonlinear magnetic force increasing the effectiveness of the EH system appears only in the ITPEH system.

Further analysis of diagrams in Figs.9-10 shows a significant advantage of the ITPEH system over the TPEH system, where a strong impact of the magnetic force due to considering additional magnet leads to generating a higher voltage output by piezo located on a vibrating beam. The RMS values of the voltage output collected in Tab.2 confirm these results. Taking these values into account, it can be concluded that tailoring potential energy in the tri-stable energy harvesting system leads to increasing the effectiveness of magnetic coupling EH systems.

In conclusion, both the numerical simulations and the experimental findings suggest that incorporating an additional fixed magnet into the conventional tri-stable energy harvesting (TPEH) system induces a nonlinear magnetic force with an increased amplitude, thereby boosts the voltage generated by the energy harvesting (EH) system. Consequently, the improved tri-stable energy harvesting (ITPEH) system, when coupled with a storage unit comprising of an optimal impedance load and a supercapacitor proves to be more efficient in powering small electrical devices with lower power demands compared to conventional TPEH systems.

Looking ahead, future studies could explore alternative methodologies for analyzing nonlinear time-series data, such as recurrence analysis [37] or the 0-1 test [38]. These approaches could provide further insights into the behavior and performance of ITPEH systems, potentially enhancing their applicability and effectiveness in various practical settings.

## REFERENCES

1. Bradai S, Naifar S, Viehweger C, Kanoun O, Litak G. Nonlinear analysis of electrodynamics broadband energy harvester. European Physical Journal. Special Topics. 2015; 224: 2919-2927.
2. Chen Y, Yan Z. Nonlinear analysis of axially loaded piezoelectric energy harvesters with flexoelectricity, International Journal of Mechanical Science. 2020;173:105473.
3. Koszewnik A, Lesniewski K, Pakrashi V. Numerical Analysis and Experimental Verification of Damage Identification Metrics for Smart Beam with MFC elements to support structural health monitoring. Sensors. 2021; 21(20): 6796.
4. Ambroziak L, Ołdziej D, Koszewnik A. Multirotor Motor Failure Detection with Piezo Sensor. Sensors. 2023; 23(2):1048.
5. Yang F, Gao M, Wang P, Zuo J, Dai J, Cong J. Efficient piezoelectric harvester for random broadband vibration of rail. Energy 2021; 218: 119559
6. Koszewnik A. Analytical Modeling and Experimental Validation of an Energy Harvesting System for the Smart Plate with an Integrated Piezo-Harvester. Sensors. 2019; 19(4): 812

Andrzej Koszewnik, Bartłomiej Ambrożkiewicz
*Enhanced Broadband Tri-Stable Energy Harvesting System by Adapting Potential Energy – Experimental Study*

DOI 10.2478/ama-2024-0066

7. Cahill P, Hazra B, Karoumi R, Mathewson A, Pakrashi V. Vibration energy harvesting based monitoring of an operational bridge undergoing forced vibration and train passage. Mechanical Systems and Signal Processing 2018; 106: 265–283.

8. Koszewnik A, Oldziej D. Amaro M., Parameter of a Magnetic Coupled Piezoelectric Energy Harvester with the homogenized Material – numerical approach and experimental study. Sensors. 2022; 22: 4073.

9. Cottone F, Vocca H, Gammaitoni L. Nonlinear. Energy harvesting. Physical Review Letters. 2009; 102.8:080601.

10. Stanton SC, McGehee CC, Mann BP. Reversible hysteresis for broadband magnetopiezoelectric energy harvesting. Applied Physical Letters. 2009;95:174103.

11. Ferrari M, Ferrari V, Guizzeti M, Trigona C. Improved energy harvesting from wideband vibrations by nonlinear piezoelectric converters. Sensors and Actuators A Physics. 2010; 162: 425-431.

12. Tang L, Yang Y. A nonlinear piezoelectric energy harvester with magnetic oscillator, Applied Physical Letters. 2012; 101: 94102.

13. Margielewicz J, Gąska D, Caban J, Litak G, Dudziak A, Ma X, Zhou S. Double-versus triple-potential well energy harvesters: dynamics and power output. Sensors 2023; 23(4): 2185.

14. Zhou S, Cao J, Inman J, Lin D. Harmonic balance analysis of nonlinear tri-stable energy harvesters for performance enhancement. Journal sound and Vibrations. 2016; 373: 223-235.

15. Zhou J, Cao D, Inman J, Lin J, Liu S, Wang Z. Broadband tristable energy harvester: modeling and experimental verification. Applied Energies. 2014; 133: 33-39.

16. Cao J, Zhou S, Wang W, Lin J. Influence of potential well depth on nonlinear tristable energy harvesting. Applied Physical Letters. 2015; 106: 173903.

17. Kim P, Seok J. Dynamic and energetic characteristics of a tri-stable magnetopiezoelastic energy harvester, Mechanical Machinery Theory. 2015; 94: 41-63.

18. Kim P, Son D, Seok J. Triple-well potential with a uniform depth: advantageous aspects in designing a multi-stable energy harvester. Applied Physcial Letters. 2016;108(24):243902

19. Kwuimy C, Woafo P, Tekam G. Analysis of tri-stable energy harvesting system having fractional order viscoelastic material. Chaos. 2015;25(1):013112.

20. Li H, Qin W, Lan C, Deng W, Zhou Z. Dynamics and coherence resonance of tri-stable energy harvesting system. Smart Material Structures. 2016;25(1):015001.

21. Cao Y, Yang J, Yang D. Coupling nonlinearities investigation and dynamic modeling of a tristable combined beam rotational energy harvesting system. Mechanical Systems and Signal Processing. 2023; 200: 110503.

22. Leng Y, Tan D, Liu J, Zhang Y, Fan S. Magnetic force analysis and performance of a tri-stable piezoelectric energy harvester under random excitations. Journal Sound and Vibrations. 2017;406:146-60.

23. Tan D, Leng YG, Gao YJ. Magnetic force of piezoelectric cantilever energy harvesters with an external magnetic field, European Physical Journal Special Topics. 2015; 224: 2839-2853.

24. Deraemaeker A, Benelechi S, Benjeddou A, Preumont A. Analytical and numerical computation of homogenized properties of MFCs: Application to a composite boom with MFC actuators and sensors. Proceedings of the III ECCOMAS thematic conference on Smart Structures and Materials. Gdansk Poland. 9–11 July 2007.

25. Deraemaeker A, Nasser H, Benjeddou A, Preumont A. Mixing Rules for the Piezoelectric Properties of Macro Fiber Composites. J. Intell. Mater. Syst. Struct. 2009; 20: 1475–1482.

26. Ksica F, Behal J, Rubes O, Hadas Z. Homogenized Model of Piezoelectric Composite Structures for Sensing Purposes. Proceedings of International Conference Mechatronics 2019: Recent Advances Towards Industry 4.0. 2019; 358-365.

27. Hu K, Li H. Large deformation mechanical modeling with bilinear stiffness for Macro-Fiber Composite bimorph based on extending mixing rules. Journal of Intelligent Material Systems and Structures. 2020; 1-13.

28. Biscani F, Nasser H, Belouettar S, Carrera E. Equivalent electroelastic properties of Macro Fiber Composite (MFC) transducers using asymptotic expansion approach, Composites. Part B. 2011; 444-455.

29. Koszewnik A. Frequency domain identification of the active 3D mechanical structure for the vibration control system, Journal of Vibroengineering. 2012; 14(2): 451-457.

30. Kletsel M, Barukin A, Amirbek D. Reed Switch and Magneto Resistor-Based Differential Protection Featuring Test Diagnostics for Converters. 2020 International Multi-Conference on Industrial Engineering and Modern Technologies. Russia. 2020; 1-6.

31. Fan K, Tan Q, Liu H, Zhang Y, Cal M. Improved energy harvesting from low-frequency small vibrations through a monostable piezoelectric energy harvester. Mechanical Systems and Signal Processing. 2019; 117: 594-608.

32. Lallart M, Anton SR, Inman DJ. Frequency self-tuning scheme for broadband vibration energy harvesting, Journal of Intelligent Material Systems and Structures. 2010; 21(9): 897-906.

33. Caban J, Litak G, Ambrożkiewicz B, Gardyński L, Stączek P, Wolszczak P. Impact-based piezoelectric energy harvesting system excited from diesel engine suspension. Applied Computer Science 2020; 16(3): 16-29.

34. Erturk A, Hoffmann J, Inman DJ, A piezomagnetoelastic structure for broadband vibration energy harvesting. Applied Physics Letters. 2009; 94(25): 254102.

35. Łępicka M, Górski G, Grądzka-Dahlke M, Litak G, Ambrożkiewicz B, Analysis of tribological behaviour of titanium nitride-coated stainless steel with the use of wavelet-based methods. Archive of Applied Mechanics. 2021; 91(11): 4475-4483.

36. Wang C, Zhang J, Zhu HP. A combined method for time-varying parameter identification based on variational mode decomposition and generalized morse wavelet. International Journal of Structural Stability and Dynamics 2020; 20(7): 2050077.

37. Syta A, Czarnigowski J, Jakliński P. Detection of cylinder misfire in an aircraft engine using linear and non-linear signal analysis. Measurement: Journal of the International Measurement Confederation. 2021; 174: 108982.

38. Litak G, Syta A, Budhraja M, Saha LM. Detection of the chaotic behaviour of a bouncing ball by the 0-1 test. Chaos. Solutions and Fractals 2009; 42(3): 1511-1517.

Andrzej Koszewnik: https://orcid.org/0000-0001-6430-6007

Bartłomiej Ambrożkiewicz: https://orcid.org/0000-0002-8288-5230